Proceedings of the Eighteenth International Conference on
Civil, Structural and Environmental Engineering Computing
Edited by: P. Iványi, J. Kruis and B.H.V. Topping
Civil-Comp Conferences, Volume 10, Paper 3.1
Civil-Comp Press, Edinburgh, United Kingdom, 2025
ISSN: 2753-3239, doi: 10.4203/ccc.10.3.1

Lattice Discrete Particle Model for Beta-Titanium Alloys

J. Kruis, J. Vorel and A. Jíra

Department of Mechanics, Faculty of Civil Engineering, Czech Technical University in Prague, Czech Republic

Abstract

This paper presents a novel numerical model based on the lattice discrete particle model to simulate the behaviour of 3D-printed alloy structures. The overall research focuses on improving implants' mechanical performance and biocompatibility, specifically addressing issues like stress shielding, bone mass loss, and implant loosening. By modelling materials at the particle scale, the lattice discrete particle model effectively captures the mesostructure of 3D-printed metals. The contribution develops two plasticity models to account for the material properties of titanium alloys. The effects of inherent porosity due to 3D printing are incorporated into the model, revealing significant performance impacts, particularly for structures close to the printing limit.

Keywords: lattice discrete particle model, 3D-printed structures, Ti25Nb4Ta8Sn alloy, volumetric-deviatoric split, isotropic damage, explicit integration methods.

1 Introduction

3D printing technology can be successfully used in joint and dental implants. The current implants are predominantly made of Ti6Al4V alloy, which suffers from a relatively high modulus of elasticity and possible release of toxic substances into the organism. Therefore, other alloys are being sought. This contribution concerns with beta-titanium alloys which are characterized by titanium's lightweight nature with excellent durability, strength, thermal stability, biocompatibility, and corrosion resistance. One such alloy is Ti25Nb4Ta8Sn, where niobium (Nb) and tantalum (Ta) stabilize the titanium in its beta structure [1] (body-centered cubic lattice–BCC/K8).

One order of magnitude lower stiffness of titanium specimens obtained from numerical simulations than experimental measurements is described in paper [2]. Such discrepancy is assigned to the flaws arising in the small scale specimens during the 3D printing. Therefore, numerical models based on the continuum theory were replaced by a numerical model based on the lattice discrete particle model (LDPM) [3], which was originally developed for simulation of concrete. LDPM can generally simulate the material of interest at the particle scale to consider their size and distribution. The material behaviour is defined at the facets between the adjacent particles. The influence of printing precision is studied too.

On each facet, the normal and two tangential strains are determined. Moreover, the volumetric and deviatoric strains are computed. With the help of volumetric and deviatoric moduli, the corresponding stresses are easily obtained. With respect to the experimental results, numerical model has to be based on elasto-plastic theory which is combined with the damage mechanics. Equivalent strains are computed on facets and simple yield condition with hardening is used. The damage is assumed to be isotropic and the linear softening law is used.

Lattice discrete particle models usually do not provide the stiffness matrix, which naturally leads to applying an explicit time integration method. The explicit methods are conditionally stable [4], and the length of the time step is relatively very small. In connection with the lattice models used to analyse 3D printed specimens, hundreds of thousands of degrees of freedom are needed. The large number of degrees of freedom and very short time steps lead to difficulties. The finite difference method, which is used, was therefore optimized. Laboratory experiments based on dogbone specimens as well as numerical simulations reveal significant dependency of the specimen performance on imperfections caused by 3D printing and on the sample thickness. The smaller thickness, the larger variation of the response. The numerical simulations without the damage theory lead to large error.

2 Lattice Discrete Particle Model

When considering the behaviour of quasi-brittle materials, including rocks [5] and concrete [3], [6], the lattice discrete particle model is typically employed, provided

that the internal structure is taken into consideration. The material is discretised as a collection of rigid entities, or cells, interacting across the defined facets that separate them. These facets, which are presumed to be between the neighbouring cells, may serve as surfaces for cracks. First, spherical particles are placed into the studied volume. With the use of a Delaunay tetrahedralization of the particle centres and nodes used to describe the exterior surface of the volume, the lattice system that represents the mesostructure topology is established. Next, the 3D tessellation is used to design the polyhedral cell system. Keep in mind that there are numerous options available for the tessellation, as discussed, for instance, in [3] and [7]. The aggregate and the matrix phase that envelops the particles are combined to create cells. In contrast to the first LDPM formulation, the current paper requires the 3D-printed metals' particle size distribution to be specified. Figure 1 shows two examples of 3D-printed alloys with different porosity.

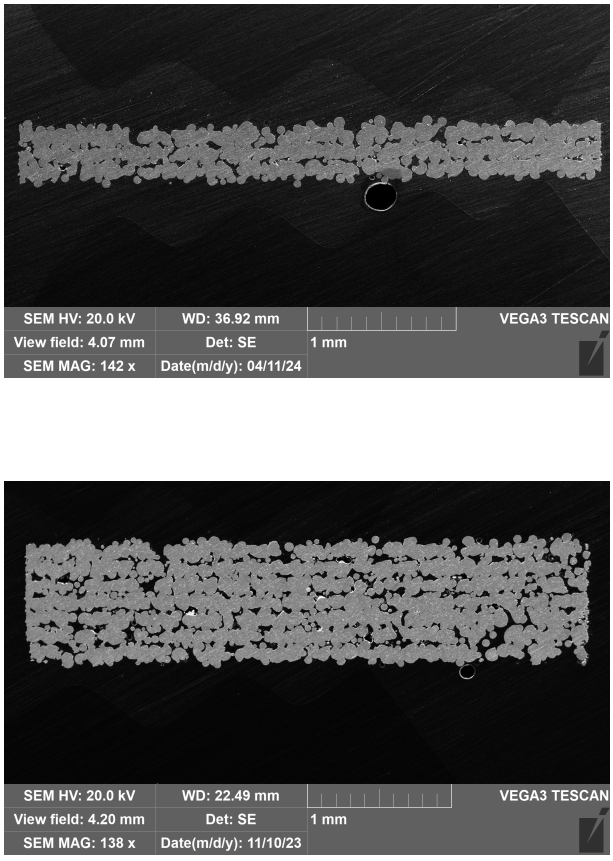

Figure 1: Printed alloys with different porosities.

The integrated defects and numerical model are displayed in Figure 2. The model definition is based on stress and strain vectors defined on the facets. The rigid body kinetics is employed to describe the displacement vector, $\underline{u}$, associated with the facets [3]

$$\underline{u}\left(\underline{x}\right) = \underline{u}_i + \underline{\theta}_i \times \left(\underline{x} - \underline{x}_i\right), \tag{1}$$

(a) (b)

Figure 2: LDPM model of dog bone specimen: (a) full model; (b) part of the model with flaws (voids) in the cross-section.

where $\underline{u}_i$ and $\underline{\theta}_i$ are the translational and rotational degrees of freedom of node i with coordinate vector $\underline{x}_i$. For the given displacements and rotations of the associated particles, the relative displacement at the centroid of facet k can be determined as

$$\underline{u}_{Ck} = \underline{u}_{Cj} - \underline{u}_{Ci}, \tag{2}$$

where $\underline{u}_{Ci}$ and $\underline{u}_{Cj}$ are the displacements at the facet centroid caused by the translations and rotations of the adjacent nodes i and j, respectively.

LDPM has proven its applicability for modelling of various materials, i.e., rocks [5] and concrete [3], as well as many engineering problems such as adhesive anchors, prestressed concrete beams, and fibre-reinforced polymer-concrete joints. Figure 2 displays the integrated defects and numerical model. The model definition is based on stress and strain vectors defined on the facets. The rigid body kinetics is employed to describe the displacement vector associated with the facets [3]. However, the original formulation is not able to recover the full Poisson ratio range ($-1 < \nu < 0.5$) and is limited to $\nu < 0.25$. Therefore, the volumetric-deviatoric split introduced in the microplane models [8] is considered. The volumetric-deviatoric split allows the recovery of the full Poisson ratio range needed for alloys and other materials. Because of the underlying tetrahedral mesh and corresponding facets Ω_e (see [3]) the volumetric (hydrostatic) strain is calculated as [9]

$$\varepsilon_{Vk} = \frac{1}{3\Omega_{e,0}} \sum_{m \in \mathcal{F}_e} \Gamma_m l_{ij} \varepsilon_{Nm}, \tag{3}$$

where $\Omega_{e,0}$ is the initial volume of the tetrahedral element, $\mathcal{F}_e$ is the set of facets belonging to one element, and Γ_m and l_{ij} are the facet area and distance of the adjacent nodes corresponding to the facet, respectively. ε_{Nm} stands for the normal strain component on the facet m. The normal deviatoric strain for facet k is written as

$$\varepsilon_{NDk} = \varepsilon_{Nk} - \varepsilon_{Vk}. \tag{4}$$

Moreover, the shear (tangential) strain in the plane of the facet is written as $\varepsilon_{Tk} = (\varepsilon_{Mk}^2 + \varepsilon_{Lk}^2)^{1/2}$, where ε_{Mk} and ε_{Lk} are the shear components in the local coordinate system. The deviatoric strain is defined as $\varepsilon_{Dk} = (\varepsilon_{NDk}^2 + \varepsilon_{Tk}^2)^{1/2}$. The corresponding stress components then read

$$\sigma_V = E_V \varepsilon_N, \quad \sigma_{ND} = E_D \varepsilon_{ND}, \quad \sigma_M = E_D \varepsilon_M, \quad \sigma_L = E_D \varepsilon_L, \tag{5}$$

where $E_V = E/(1-\nu)$ and $E_D = E/(1+\nu)$ are the volumetric and deviatoric moduli, respectively, related to Young's modulus E. The constitutive material law defined on the facets is described in the following section. By imposing the equilibrium through the principle of virtual work, the internal work and nodal forces associated with the facet can be calculated [3]. Note that subscript k is omitted in the following text for readability.

3 LDPM for Elastoplasticity

This section introduces a lattice discrete particle model for plasticity. The model is based on the volumetric-deviatoric split, and the approaches outlined in [10]. This equivalent stress-based material model is implemented in MARS software[1] and SIFEL software[2] and is also combined with isotropic damage. The model is defined by means of equivalent stress, σ^{eq}, and strain, $\varepsilon^{\mathsf{eq}}$. The equivalent strain has the form

$$\varepsilon^{\mathsf{eq}} = \sqrt{(\varepsilon_V + \alpha\varepsilon_{ND})^2 + \alpha\,(\varepsilon_M^2 + \varepsilon_L^2)} = \sqrt{(\varepsilon_N^{\mathsf{eq}})^2 + \alpha\varepsilon_T^2}, \tag{6}$$

where $\varepsilon_N^{\mathsf{eq}} = \varepsilon_V + \alpha\varepsilon_{ND}$, α stands for the interaction coefficient. This definition of equivalent normal strain originates from the assumption that $\sigma_N = E_V \varepsilon_N^{\mathsf{eq}}$. Based on the principle of virtual power, we relate the stress components to the equivalent stress as

$$\sigma_N = \sigma^{\mathsf{eq}} \frac{\varepsilon_N^{\mathsf{eq}}}{\varepsilon^{\mathsf{eq}}}, \quad \sigma_M = \sigma^{\mathsf{eq}} \frac{\alpha\varepsilon_M}{\varepsilon^{\mathsf{eq}}}, \quad \sigma_L = \sigma^{\mathsf{eq}} \frac{\alpha\varepsilon_L}{\varepsilon^{\mathsf{eq}}}, \tag{7}$$

and

$$\sigma_V = \sigma^{\mathsf{eq}} \frac{\varepsilon_V}{\varepsilon^{\mathsf{eq}}}, \quad \sigma_{ND} = \sigma^{\mathsf{eq}} \frac{\alpha\varepsilon_{ND}}{\varepsilon^{\mathsf{eq}}}. \tag{8}$$

By substituting Equations (7) and (8) into (6), the effective stress is obtained in terms of normal and shear stresses

$$\sigma^{\mathsf{eq}} = \sqrt{\sigma_N^2 + \frac{\sigma_T^2}{\alpha}}, \quad \sigma_T = \sqrt{\sigma_M^2 + \sigma_L^2}. \tag{9}$$

If the elastic behaviour is assumed and taking into account Equations (7) and (8), the stresses are written as

$$\sigma_V = E^{\mathsf{eq}} \varepsilon_V, \quad \sigma_{ND} = \alpha E^{\mathsf{eq}} \varepsilon_{ND}, \quad \sigma_M = \alpha E^{\mathsf{eq}} \varepsilon_M, \quad \sigma_L = \alpha E^{\mathsf{eq}} \varepsilon_L, \tag{10}$$

[1] https://www.es3inc.com/mars-solver/

[2] https://mech.fsv.cvut.cz/∼sifel/

where $E^{\mathsf{eq}} = \sigma^{\mathsf{eq}}/\varepsilon^{\mathsf{eq}} = E_V$ and thus $\alpha = E_D/E_V = 1 - 2\nu/1 + \nu$. This formulation covers the whole physical range of the Poisson ratio.

In this model, the yield condition is written as

$$f\left(\underline{\sigma}\right) = \left(\sigma^{\mathsf{eq}}\right)^2 - \left[\sigma_Y\left(\kappa\right)\right]^2 = 0, \tag{11}$$

where κ is the hardening variable, which is related to the plastic multiplier λ through the relation $\dot{\kappa} = \dot{\lambda}$ and yield strength

$$\sigma_Y\left(\kappa\right) = \sigma_{Y0} + H\kappa, \tag{12}$$

where σ_{Y0} is the initial yield stress and H is the hardening modulus. When this condition is satisfied, yielding occurs. The radial return is performed on the equivalent stress if $f\left(\underline{\sigma}\right) > 0$.

If the elastoplastic model is combined with the isotropic damage, the final stresses are evaluated as

$$\sigma_N = (1-\omega)\sigma_N, \quad \sigma_M = (1-\omega)\sigma_M, \quad \sigma_L = (1-\omega)\sigma_L, \tag{13}$$

where ω is the damage parameter. The linear softening law is assumed and defined in the form

$$\omega = \frac{\kappa - \kappa_0}{\kappa_f - \kappa_0}, \tag{14}$$

where $\kappa_f = l_f/l_{ij}$, l_f is fracture opening, and κ_0 stands for the damage threshold (onset of damage).

4 Preliminary Results

This section summarizes the preliminary findings of the above-described numerical model based on the equivalent stress and volume of pores equal to 15% assumed. The material model parameters used to simulate the uniaxial loading of dogbone specimens are summarised in Table 1. The results obtained for the model with and without damage are presented in Figure 3(a). As can be seen from the presented results, the inserted pores reduced the yield strength of the specimen compared to the raw material. Moreover, the material model with damage is capable of capturing the specimen's failure and crack evolution, see Figure 3(b).

E [GPa]	ν [-]	σ_{Y0} [MPa]	H [GPa]	κ_0 [-]	l_f [mm]
120	0.3	750	4.4	0.001	0.2

Table 1: Material properties used in current study for titanium alloy

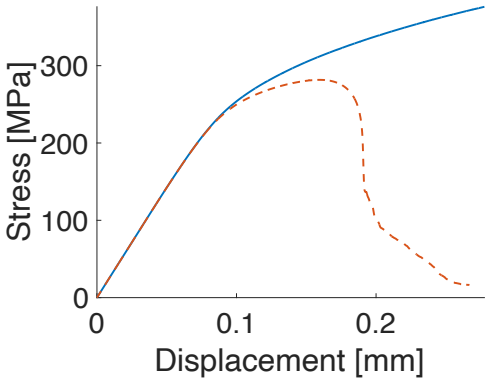

(a)

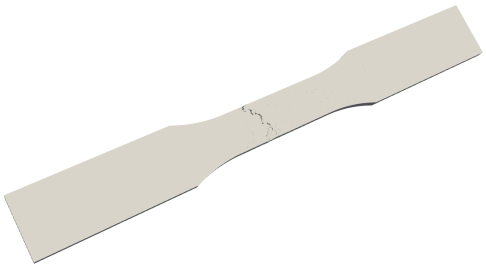

(b)

Figure 3: Uniaxial tension of dog bone specimen: (a) load-displacement diagram - model without damage (solid line); model with damage (dashed line); (b) crack evolution in laboratory specimen.

5 Conclusion

The paper introduces a novel lattice discrete particle model for 3D-printed titanium alloys. By removing cells from the computational model, the intrinsic porosity caused by the printing procedure is taken into account. It's important to note that the imperfections caused by the printing procedure significantly influence the specimen performance, particularly for smaller thicknesses near the printing limits. This research is significant as it presents a numerical model for a deeper understanding of the factors that affect the performance of 3D-printed titanium alloys.

Acknowledgement: The financial support provided by the GAČR grant No. 23-04971S is gratefully acknowledged.

References

[1] I. Jirka, M. Vandrovcová, O. Frank, Z. Tolde, J. Plšek, T. Luxbacher, L. Bačáková, V. Starý, "On the role of Nb-related sites of an oxidized β-TiNb alloy

surface in its interaction with osteoblast-like MG-63 cells", Materials Science and Engineering C, 33, 1636-1645, 2013.

[2] A. Jíra, M. Šejnoha, T. Krejčí, J. Vorel, L. Řehounek, G. Marseglia, "Mechanical properties of porous structures for dental implants: Experimental study and computational homogenization", Materials, vol. 14, no. 16, p. 4592, 2021.

[3] G. Cusatis, D. Pelessone, A. Mencarelli, "Lattice discrete particle model (LDPM) for failure behavior of concrete. I: Theory", Cement and Concrete Composites, vol. 33, n. 9, 881-890, 2011.

[4] K.J. Bathe, Finite Element Procedures, Prentice Hall, USA, 1996, 2nd edition [K.J. Bathe], Watertown, MA, USA, 2014.

[5] S.R. Ashari, G. Buscarnera, G. Cusatis, "A lattice discrete particle model for pressure-dependent inelasticity in granular rocks", International Journal of Rock Mechanics and Mining Sciences, 91, 49–58, 2017.

[6] G. Cusatis, A. Mencarelli, D. Pelessone, J. Baylot, "Lattice discrete particle model (LDPM) for failure behavior of concrete. II: Calibration and validation", Cement and Concrete Composites, vol. 33, n. 9, 891–905, 2011.

[7] J. Eliáš, "Boundary layer effect on behavior of discrete models", Materials, vol. 10, n. 2, 2017.

[8] I. Carol, Z.P. Bažant, "Damage and plasticity in microplane theory", International Journal of Solids and Structures, vol. 34, n. 29, 3807–3835, 1997.

[9] G. Cusatis, R. Rezakhani, E.A. Schauffert, "Discontinuous Cell Method (DCM) for the simulation of cohesive fracture and fragmentation of continuous media", Engineering Fracture Mechanics, 170, 1–22, 2017.

[10] M. Brocca, Z.P. Bažant, "Microplane constitutive model and metal plasticity", Applied Mechanics Reviews, vol. 53, n. 10, 265–281, 2000.